A New Linear Tricobalt Compound with Di(2-pyridyl)amide (dpa) Ligands: Two-Step Spin Crossover of $[Co_3(dpa)_4Cl_2][BF_4]$

Rodolphe Clérac,[†] F. Albert Cotton,*[,†] Kim R. Dunbar,*[,†] Tongbu Lu,[†,‡] Carlos A. Murillo,*[,†,§] and Xiaoping Wang[†]

Contribution from The Laboratory for Molecular Structure and Bonding, Department of Chemistry, Texas A&M University, P.O. Box 30012, College Station, Texas 77842-3012, and Department of Chemistry, University of Costa Rica, Ciudad Universitaria, Costa Rica

Received November 18, 1999

Abstract: Chemical oxidation of the linear tricobalt compound $Co_3(dpa)_4Cl_2$ (**1**) with 1 equiv of $NOBF_4$ yields the one-electron oxidized species $[Co_3(dpa)_4Cl_2]^+$ ($\mathbf{1}^+$), which crystallizes from dichloromethane as a solvate $[Co_3(dpa)_4Cl_2][BF_4]\cdot 2CH_2Cl_2$ ($\mathbf{2}\cdot 2CH_2Cl_2$). The crystal structure of $\mathbf{2}\cdot x CH_2Cl_2$ (with x varying from 1.125 to 2.0) has been determined at 100, 213, and 300 K, showing very little variation and an essentially symmetrical arrangement of three Co atoms in the cation $\mathbf{1}^+$ with Co−Co distances of 2.3168(8) and 2.3289(8) Å. The terminal cobalt to axial chloride distances are 2.350(1) and 2.376(1) Å at 100 K. The cation maintains its symmetrical structure at ambient temperature (300 K) with only a slight lengthening (0.01−0.02 Å) of Co−Co and Co−N distances. Temperature studies of the magnetic properties for **2** in both solution and solid state have revealed a spin-crossover behavior occurring in two gradual steps, indicating that **2** exhibits a diamagnetic ground state and thermally accessible triplet and quintet spin states. An ideal solution model taking into account the two equilibria ($S = 0 \leftrightarrow S = 1$ and $S = 1 \leftrightarrow S = 2$) has been used to fit the magnetic data. The derived enthalpy and the entropy changes associated with the two steps have been found in solution to be $\Delta H_1 = 8.7$ kJ mol^{-1}, $\Delta S_1 = 43$ J mol^{-1} K^{-1} and $\Delta H_2 = 22.8$ kJ mol^{-1}, $\Delta S_2 = 81$ J mol^{-1} K^{-1}, and in the solid state to be $\Delta H_1 = 3.6$ kJ mol^{-1}, $\Delta S_1 = 11$ J mol^{-1} K^{-1} and $\Delta H_2 = 17.4$ kJ mol^{-1}, $\Delta S_2 = 53$ J mol^{-1} K^{-1}. The characteristic temperatures of the spin crossover can be estimated from the above thermodynamic parameters ($T_{sc} = \Delta H/\Delta S$) as $T_{sc1} = 201$ K and $T_{sc2} = 281$ K in solution and $T_{sc1} = 315$ K and $T_{sc2} = 330$ K in the solid state. The shape of the magnetic curves do not include a plateau for an intermediate spin state, and characteristic temperatures are very close to each other. These facts point to the conclusion that the thermal population of the triplet and quintet states occurs quasi-simultaneously. To the best of our knowledge, this paper reports the first example of a two-step spin crossover in a Co compound.

Introduction

Compounds of the type $M_3(dpa)_4X_2$, where dpa is the anion of di-2-pyridylamine (**I**), X is a monoanion, and M = Co,[1,2] Cr,[3] Cu,[4] Ni,[5] Rh,[6] and Ru,[6] have been recently reported. Except for M = Cr, and occasionally Co, a symmetrical arrangement of the three metal atoms in the $M_3(dpa)_4X_2$ molecules is found. Molecules with a trichromium[3] or tricobalt[1,2] core may be symmetrical or unsymmetrical, depending on the composition of the crystal and the nature of the axial ligands. The tendency for the chromium chains to form unsymmetrical molecules has been attributed to the favorable formation of a quadruple bond between two d^4 Cr^{2+} atoms, which leaves the third Cr^{2+} atom in a five-coordinate square-pyramidal environment. The one-electron oxidation of the Cr_3^{6+} core to Cr_3^{7+} produces only unsymmetrical $[Cr_3(dpa)_4Cl_2]^+$ species,[3] in which the terminal Cr^{3+} ion is isolated from the metal−metal bonded dichromium unit.

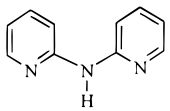

Hdpa (**I**)

A rather subtle difference exists between the symmetrical and unsymmetrical structures of $Co_3(dpa)_4Cl_2$ (**1**). They can be isolated as crystals of different composition from dichloromethane solution, namely $\mathbf{1}\cdot CH_2Cl_2$ and $\mathbf{1}\cdot 2CH_2Cl_2$. These

* To whom correspondence should be addressed. E-mail: cotton@tamu.edu; murillo@tamu.edu.

† Texas A&M University.

‡ Presently at Zhongshan University, Guangzhou, 510275, China.

§ University of Costa Rica.

(1) (a) Cotton, F. A.; Murillo, C. A.; Wang, X. *J. Chem. Soc., Dalton Trans*. **1999**, 3327−3328. (b) Cotton, F. A.; Daniels, L. M.; Jordan, G. T., IV *Chem. Commun*. **1997**, 421−422. (c) Cotton, F. A.; Daniels, L. M.; Jordan, G. T., IV; Murillo, C. A. *J. Am. Chem. Soc*. **1997**, *119*, 10377−10381.

(2) Yang, E.; Cheng, M.; Tsai, M.; Peng, S. M. A. *J. Chem. Soc., Chem. Commun*. **1994**, 2377−2378.

(3) (a) Cotton, F. A.; Daniels, L. M.; Murillo, C. A.; Pascual, I. *J. Am. Chem. Soc*. **1997**, *119*, 10223−10224. (b) Cotton, F. A.; Daniels, L. M.; Pascual, I. *Inorg. Chem. Commun*. **1998**, *1*, 1−3. (c) Clérac, R.; Cotton, F. A.; Daniels, L. M.; Dunbar, K. R.; Murillo, C. A.; Pascual, I. *Inorg. Chem*. **2000**, *39*, 752−756.

(4) (a) Wu, L.-P.; Field, P.; Morrissey, T.; Murphy, C.; Nagle, P.; Hathaway, B.; Simmons, C.; Thornton, P. *J. Chem. Soc., Dalton Trans*. **1990**, 3835−3840. (b) Pyrka, G. J.; El-Mekki, M.; Pinkerton, A. A. *J. Chem. Soc., Chem. Commun*. **1991**, 84−85.

(5) (a) Aduldecha, S.; Hathaway, B. *J. Chem. Soc., Dalton Trans*. **1991**, 993−998. (b) Clérac, R.; Cotton, F. A.; Dunbar, K. R.; Murillo, C. A.; Pascual, I.; Wang, X. *Inorg. Chem*. **1999**, *38*, 2655−2657.

(6) Sheu, J.-T.; Lin, C.-C.; Chao, I.; Wang, C.-C.; Peng, S.-M. *Chem. Commun*. **1997**, 315−316.

10.1021/ja994051b CCC: $19.00
Published on Web 02/18/2000

Scheme 1

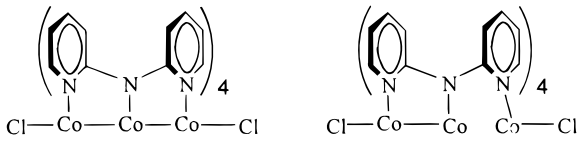

***s*-$Co_3(dpa)_4Cl_2$** ***u*-$Co_3(dpa)_4Cl_2$**

contain symmetrical and unsymmetrical clusters, respectively.[1a] The former has a delocalized metal−metal bond over the three cobalt atoms.[7] In **1**·$2CH_2Cl_2$, the $Co_3(dpa)_4Cl_2$ molecule has a single bond between two of the metal atoms, while the third cobalt is not involved in metal−metal bonding. The symmetrical and unsymmetrical molecules of **1**, abbreviated here as *s*-**1** and *u*-**1** (Scheme 1), represent a pair of well-defined bond stretch isomers.[8] In the solid state, both isomers exhibit a doublet ground state at low temperatures. Upon increasing the temperature, both compounds exhibit a gradual one-step spin crossover to a higher spin state. Because the spin-crossover process is incomplete when the sample begins to lose solvent molecules at 350 K, it is difficult to unambiguously assign the nature of the high spin state ($S = 3/2$ or $S = 5/2$).[9]

To gain more insight into these spin-crossover phenomena, we have carried out more studies on compound **1**. The reaction of **1** with $NOBF_4$ yields $[Co_3(dpa)_4Cl_2][BF_4]$ (**2**), which contains the one electron-oxidized form of **1** as the cation $\mathbf{1}^+$. An investigation of the magnetic properties of **2** in solution by NMR spectroscopy and in the solid state by magnetic susceptibility measurements revealed spin-crossover behavior that occurs in two gradual steps. To the best of our knowledge, this compound provides the first example of a two-step spin-crossover behavior in a cobalt system. In this paper, we describe this unique compound and report its structural and physical properties.

Experimental Section

General. Manipulations were performed under an atmosphere of argon using standard Schlenk techniques. Solvents were purified by conventional methods and were freshly distilled under nitrogen prior to use. Anhydrous $CoCl_2$ was purchased from Strem Chemicals, Inc. Di-(2-pyridyl)amine was purchased from Aldrich and sublimed prior to use; $Co_3(dpa)_4Cl_2$ (**1**) was prepared according to a published procedure.[1]

Physical Measurements. ^{1}H NMR spectra of **2** were recorded on a Varian UNITY Plus 300 instrument at 300 MHz, with chemical shifts being referenced to CD_2Cl_2 (5.32 ppm). Magnetic susceptibility measurements in CH_2Cl_2 solution were performed by the Evans method.[10] The concentration of **2** at each temperature was corrected for the differences in the density of CH_2Cl_2.[11] The electronic absorption spectra were measured on a Cary 17 spectrophotometer. X-band EPR spectra in frozen dichloromethane solution were recorded on a Bruker model ESP 300 spectrometer. The magnetic susceptibility data in the solid state were collected on a Quantum Design, model MPMS-5, SQUID (superconducting quantum interference device) housed in the Department of Physics and Astronomy at Michigan State University; data were collected from 1.8 to 350 K at a field of 10 000 G. The magnetic susceptibility data were corrected for the sample holder contribution and for the intrinsic diamagnetic contribution, which was estimated experimentally at 8.6×10^{-4} emu CGS mol^{-1}. This value is in excellent agreement with the calculated one, 6.1×10^{-4} emu CGS mol^{-1}, from Pascal's constants.[12] Cyclic voltammetry was performed in dichloromethane solution with a BAS model 100 scanning potentiostat using Pt working and auxiliary electrodes and 0.1 M TBAH ([*n*-Bu_4N][PF_6]) as the supporting electrolyte. Potentials are referenced to the ferrocene/ferrocenium (Fc/Fc^+) couple, which occurs at $E_{1/2} = +0.44$ V versus Ag/AgCl. The values of $E_{1/2}$ were taken as $(E_{pa} + E_{pc})/2$, where E_{pa} and E_{pc} are the anodic and cathodic peak potentials, respectively. Elemental analyses performed by Canadian Microanalytical Services gave satisfactory results.

Preparation of $[Co_3(dpa)_4Cl_2][BF_4]$·$x$$CH_2Cl_2$ (2·$x$$CH_2Cl_2$). A solution of $NOBF_4$ (0.039 g, 0.33 mmol) in CH_2Cl_2 (20 mL) was added slowly with stirring to a flask containing a solution of **1** (0.31 g, 0.30 mmol) in CH_2Cl_2 (10 mL), to produce a deep green solution. The reaction mixture was stirred for an additional 1 h, filtered, and concentrated to 15 mL. After layering with hexanes, the solution yields crystals of **2**·$x$$CH_2Cl_2$ in approximately 1 week. These were collected and washed with hexanes. Yield: 0.32 g, 92%. ^{1}H NMR (CD_2Cl_2, rt): δ 38.56, 23.12, 3.04, −11.02. IR (KBr, cm^{-1}) 1600 (s), 1550 (w), 1464 (s), 1425 (s), 1357 (m), 1367 (m), 1308 (s), 1283 (m), 1261 (w), 1225 (s), 1156 (s), 1084 (s), 1055 (s), 1024 (s), 884 (sh), 865 (s), 803 (w), 765 (s), 740 (m), 699 (w), 670 (w), 649 (w), 624 (w), 533 (w), 514 (m), 463 (w), 431 (w), 396 (m). UV/vis/near-IR (nm, ϵ/M^{-1} cm^{-1}): 292 (56310), 431 (sh, 5300), 478 (sh, 2520), 720 (br, sh, 2650), 762 (2440), 850 (sh, 1398), 1175 (br, 1152). Anal. Calcd for $C_{41.5}H_{35}B_1Cl_5Co_3F_4N_{12}$ (**2**·$1.5CH_2Cl_2$): C, 43.63; H, 3.09; N, 14.70. Found: C, 43.47; H, 3.27; N, 14.33.

X-ray Crystallography. Three crystals of **2**·$x$$CH_2Cl_2$ were used for data collection at temperatures of 100, 213, and 300 K. Each crystal was mounted on a quartz fiber with a small amount of silicone grease and transferred to a goniometer head. Geometric and intensity data sets at 213 and 300 K were gathered on a Nonius FAST area detector system, utilizing the software program MADNES.[13] Cell parameters for FAST data were obtained from an autoindexing routine and were refined with 250 strong reflections in the 2θ range 18.1−41.6°. Cell dimensions and Laue symmetry for all crystals were confirmed from axial photographs. All data were corrected for Lorentz and polarization effects. Intensity data were transferred into SHELX format using the program PROCOR.[14]

Data for **2**·$x$$CH_2Cl_2$ at 100 K were collected on a Bruker SMART 1000 CCD detector system equipped with a liquid nitrogen low-temperature controller. Cell parameters were obtained using SMART[15] software. Data were corrected for Lorentz and polarization effects using the program SAINTPLUS.[16] Absorption corrections were applied using SADABS.[17]

For each of the three data sets the positions of the heavy atoms were found by the direct methods program in SHELXTL.[18] Subsequent cycles of least-squares refinement followed by difference Fourier syntheses revealed the positions of the remaining non-hydrogen atoms. The interstitial dichloromethane molecules were found to be disordered, and

(7) Rohmer, M.-M.; Bénard, M. *J. Am. Chem. Soc*. **1998**, *120*, 9372−9373.

(8) (a) Parkin, G.; Hoffmann, R. *Angew. Chem., Int. Ed. Engl*. **1994**, *33*, 1462. (b) Parkin, G. *Chem. Rev*. **1993**, *93*, 887−911. (c) Parkin, G. *Acc. Chem. Res*. **1992**, *25*, 455−460.

(9) Clérac, R.; Cotton, F. A.; Daniels, L. M.; Dunbar, K. R.; Kirschbaum, K.; Murillo, C. A.; Pinkerton, A. A.; Schultz, A. J.; Wang, X. Manuscript in preparation.

(10) (a) Evans, D. F. *J. Chem. Soc*. **1959**, 2003−2005. (b) Live, D. H.; Chan, S. I. *Anal. Chem*. **1970**, *42*, 791−792. (c) Ostfeld, D.; Cohen I. A. *J. Chem. Educ*. **1972**, *49*, 829. (d) Schubert, E. M. *J. Chem. Educ*. **1992**, *69*, 62.

(11) Yaws, C. L. *Thermodynamic and Physical Property Data*; Gulf Publishing Company: Houston, 1992.

(12) Boudreaux, E. A.; Mulay, L. N., Eds. *Theory and Applications of Molecular Paramagnetism.* John Wiley & Sons: New York, 1976.

(13) Pflugrath, J.; Messerschmitt, A. *MADNES*, Munich Area Detector (New EEC) System, Version EEC 11/1/89, with enhancements by Enraf-Nonius Corp., Delft, The Netherlands. A description of MADNES appears: Messerschmitt, A.; Pflugrath, J. *J. Appl. Crystallogr*. **1987**, *20*, 306−315.

(14) (a) Kabsch, W. *J. Appl. Crystallogr*. **1988**, *21*, 67−71. (b) Kabsch, W. *J. Appl. Crystallogr*. **1988**, *21*, 916−924.

(15) *SMART V5.05 Software for the CCD Detector System*; Bruker Analytical X-ray Systems, Inc., Madison, WI, 1998.

(16) *SAINTPLUS, V5.00 Software for the CCD Detector System*; Bruker Analytical X-ray Systems, Inc., Madison, WI, 1998.

(17) *SADABS*. Program for absorption correction using SMART CCD based on the method of Blessing: Blessing, R. H. *Acta Crystallogr*. **1995**, *A51*, 33−38.

(18) *SHELXTL, Version 5.03*; Siemens Industrial Automation Inc., Madison, WI, 1994.

Table 1. Crystallographic Data for $[Co_3(dpa)_4Cl_2][BF_4]\cdot xCH_2Cl_2$ (**2**)

formula	$C_{41.5}H_{35}B_1Cl_5Co_3F_4N_{12}$	$C_{42}H_{36}B_1Cl_6Co_3F_4N_{12}$	$C_{41.125}H_{34.25}B_1Cl_{4.25}Co_3F_4N_{12}$
formula weight	1142.67	1185.13	1110.82
temperature, K	100(2)	213(2)	300(2)
crystal system	monoclinic	monoclinic	monoclinic
space group	$P2_1/n$	$P2_1/n$	$P2_1/n$
a, Å	11.3249(7)	11.399(7)	11.325(1)
b, Å	20.759(1)	20.913(1)	20.915(2)
c, Å	19.422(1)	19.752(1)	19.786(1)
β, deg	93.061(1)	92.954(3)	92.951(6)
V, Å^3	4559.3(5)	4702.7(4)	4680.3(7)
Z	4	4	4
D_{calc}, g cm^{-3}	1.665	1.674	1.576
R_1[a], wR_2[b] [$I > 2\sigma(I)$]	0.061, 0.134	0.057, 0.123	0.067, 0.154
R_1[a], wR_2[b] (all data)	0.083, 0.148	0.069, 0.144	0.085, 0.171
quality-of-fit[c]	1.107	1.067	1.054

[a] $R_1 = \sum||F_o| - |F_c||/\sum|F_o|$. [b] $wR_2 = [\sum[w(F_o^2 - F_c^2)^2]/\sum[w(F_o^2)^2]]^{1/2}$. [c] Quality-of-fit $= [\sum[w(F_o^2 - F_c^2)^2]/(N_{obs} - N_{params})]^{1/2}$, based on all data.

the occupancy of the solvent molecules also varied as a result of solvent loss. The data set at 213 K was obtained by using a crystal that was mounted on the goniometer head immediately after it was removed from the solution. Final refinement gave the composition $[Co_3(dpa)_4Cl_2][BF_4]\cdot 2CH_2Cl_2$. The crystals used for the other two data sets were cut from larger crystals that had been separated from the mother liquor. The quantities of interstitial dichloromethane per tricobalt unit was found to be 1.5 for data collected at 100 K and 1.125 for data at 300 K. Though partial loss of solvent molecules had been observed, the crystal system of **2** did not change, and the structures were all successfully refined in space group $P2_1/n$. Other details of data collection and refinement are given in Table 1. Selected distances and angles are listed in Table 2.

Results and Discussions

Electrochemical and Spectroscopic Properties. Compound **1** was investigated by cyclic voltammetry and differential pulse voltammetry; the results are shown in Figure 1. The cyclic voltammogram of **1** displays two reversible one-electron waves at $E_{1/2}(ox)_1 = +0.32$ V, $E_{1/2}(ox)_2 = +1.24$ V in the range +1.5 to −0.1 V. The $E_{1/2}$ values are independent of scan rates in the range 25−1000 mV s^{-1}, as judged by the fact that the peak current is proportional to the square root of the scan rate, as expected for a reversible process. The currents associated with the two oxidations in the differential pulse voltammogram (Figure 1b) are essentially the same, consistent with the same number of electrons being involved in each of the oxidation steps. Chemical oxidation of **1** with $NOBF_4$ in dichloromethane solution gives $\mathbf{1}^+$ as $[Co_3(dpa)_4Cl_2][BF_4]$ (**2**) (eq 1):

$$Co_3(dpa)_4Cl_2 + NOBF_4 \rightarrow [Co_3(dpa)_4Cl_2][BF_4] + NO(g) \quad (1)$$

The resulting dark green solution was filtered and the filtrate was layered with hexanes to give rectangular block-shaped crystals of $\mathbf{2}\cdot x CH_2Cl_2$. Chemical oxidation to the two-electron oxidized species $\mathbf{1}^{2+}$ has not yet been achieved.

Electronic absorption spectra of compounds **1** and **2**, shown in Figure 2, are clearly different. As the result of oxidation, compound **2** has developed several new features in its electronic spectrum in the visible and near-IR region, namely a shoulder at 431 nm (23 202 cm^{-1}) and red-shifted bands located at 720 nm (13 889 cm^{-1}), 762 nm (13 123 cm^{-1}), 850 nm (11 765 cm^{-1}), and 1175 nm (8510 cm^{-1}) as broad and overlapping peaks. The original band at 568 nm (17 606 cm^{-1}) for the neutral molecule of **1** is not observed after oxidation.

Compound **2** is EPR-silent at low temperature (4.2 K) in both the solid state and solution, as expected for a singlet ground state. Between 65 and 90 K, a very broad resonance ($\Delta H =$ 4000 G) is observed at a g value of 1.94(5) (the breadth of the line precludes a more accurate determination of the g factor). At higher temperatures, the resonance continues to broaden and disappears. The ^{1}H NMR spectrum of **2** at room temperature, shown in Figure 3, consists of four peaks for the dpa ligands; these are centered at 38.56, 23.12, 3.04, and −11.02 ppm. The breadth and large shifts of the proton resonance signals are consistent with the paramagnetism of **2** at room temperature. The positions of the ^{1}H NMR signals for $\mathbf{1}^+$ are shifted far upfield from those of the neutral compound **1**, which were found at 47.96, 33.21, 15.96, and 16.78 ppm.[19] There are 32 protons for the eight pyridyl groups of the four dpa ligands in $[Co_3(dpa)_4$-

Table 2. Selected Distances (Å) and Angles (deg) for $[Co_3(dpa)_4Cl_2]^+$ ($\mathbf{1}^+$) at 100, 213, and 300 K

	100 K	213 K	300 K
Co(1)−Cl(1)	2.350(1)	2.366(2)	2.356(2)
Co(1)−Co(2)	2.3168(8)	2.321(1)	2.325(1)
Co(2)−Co(3)	2.3289(8)	2.327(1)	2.341(1)
Co(3)−Cl(2)	2.376(1)	2.378(2)	2.370(2)
Co(1)−N(1)	1.976(4)	1.985(5)	1.989(5)
Co(1)−N(4)	1.972(4)	1.979(5)	1.990(5)
Co(1)−N(7)	1.973(4)	1.971(5)	1.989(5)
Co(1)−N(10)	1.980(4)	1.985(5)	1.986(5)
Co(2)−N(2)	1.868(4)	1.867(5)	1.869(5)
Co(2)−N(5)	1.870(3)	1.884(4)	1.886(4)
Co(2)−N(8)	1.864(3)	1.873(4)	1.870(4)
Co(2)−N(11)	1.874(3)	1.877(4)	1.879(5)
Co(3)−N(3)	1.974(4)	1.976(5)	1.999(5)
Co(3)−N(6)	1.989(4)	1.978(5)	2.006(5)
Co(3)−N(9)	1.972(3)	1.980(5)	1.985(5)
Co(3)−N(12)	1.980(3)	1.984(5)	1.992(5)
Co(1)−Co(2)−Co(3)	179.22(3)	179.52(4)	179.39(4)
Co(2)−Co(1)−Cl(1)	179.58(4)	178.76(5)	179.44(6)
Co(2)−Co(3)−Cl(2)	179.47(4)	179.43(5)	179.75(6)
N(1)−Co(1)−N(4)	169.3(1)	169.0(2)	169.0(2)
N(1)−Co(1)−N(7)	88.2(2)	87.7(2)	88.8(2)
N(1)−Co(1)−N(10)	90.6(2)	92.3(2)	90.5(2)
N(4)−Co(1)−N(7)	89.7(2)	89.3(2)	89.3(2)
N(4)−Co(1)−N(10)	89.7(2)	88.9(2)	89.5(2)
N(7)−Co(1)−N(10)	170.5(2)	170.5(2)	170.4(2)
N(2)−Co(2)−N(5)	179.4(2)	179.5(2)	179.1(2)
N(2)−Co(2)−N(8)	90.0(2)	90.4(2)	90.2(2)
N(2)−Co(2)−N(11)	90.1(2)	90.1(2)	89.7(2)
N(5)−Co(2)−N(8)	89.4(2)	89.1(2)	89.3(2)
N(5)−Co(2)−N(11)	90.5(2)	90.4(2)	90.9(2)
N(8)−Co(2)−N(11)	179.8(1)	179.4(2)	179.8(2)
N(3)−Co(3)−N(6)	169.4(2)	169.7(2)	168.6(2)
N(3)−Co(3)−N(9)	88.2(2)	88.7(2)	88.0(2)
N(3)−Co(3)−N(12)	89.6(2)	89.4(2)	89.8(2)
N(6)−Co(3)−N(9)	88.9(2)	88.9(2)	89.3(2)
N(6)−Co(3)−N(12)	91.4(2)	91.1(2)	90.6(2)
N(9)−Co(3)−N(12)	169.0(2)	169.3(2)	168.2(2)

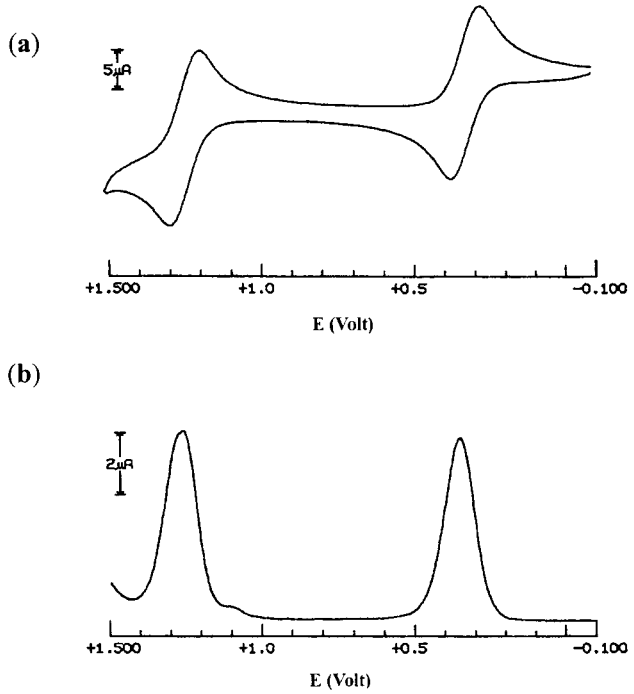

Figure 1. Cyclic voltammogram (CV) (a) and differential pulse voltammogram (DPV) (b) of **1** in dichloromethane solution.

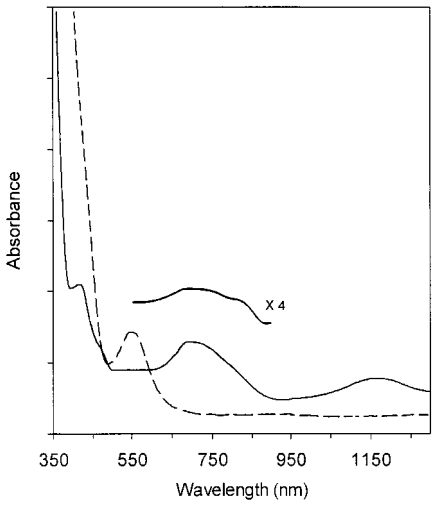

Figure 2. Electronic absorption spectrum of **2** in CH_2Cl_2 solution (solid line). The spectrum of the parent neutral molecule **1** is shown for comparison as dashed lines.

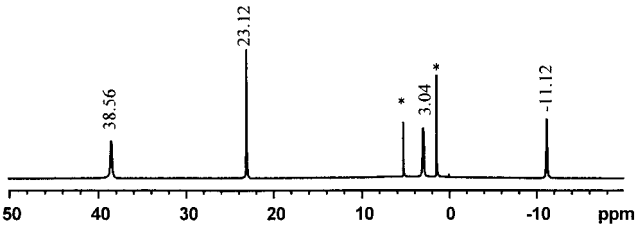

Figure 3. ^{1}H NMR spectrum of **2** in CD_2Cl_2 at ambient temperature. The starred peaks are solvent signals.

$Cl_2]^+$ (**1**$^+$). For the symmetrical structure with idealized D_4 symmetry, there should be only four signals, whereas, if the molecule exhibited lower symmetry in solution, as it would if the middle Co atom were to move off center, at least twice as many signals would appear. Clearly, the NMR spectrum tells us that, in the solution structure, all eight pyridyl rings in **1**$^+$ are equivalent on the NMR time scale.

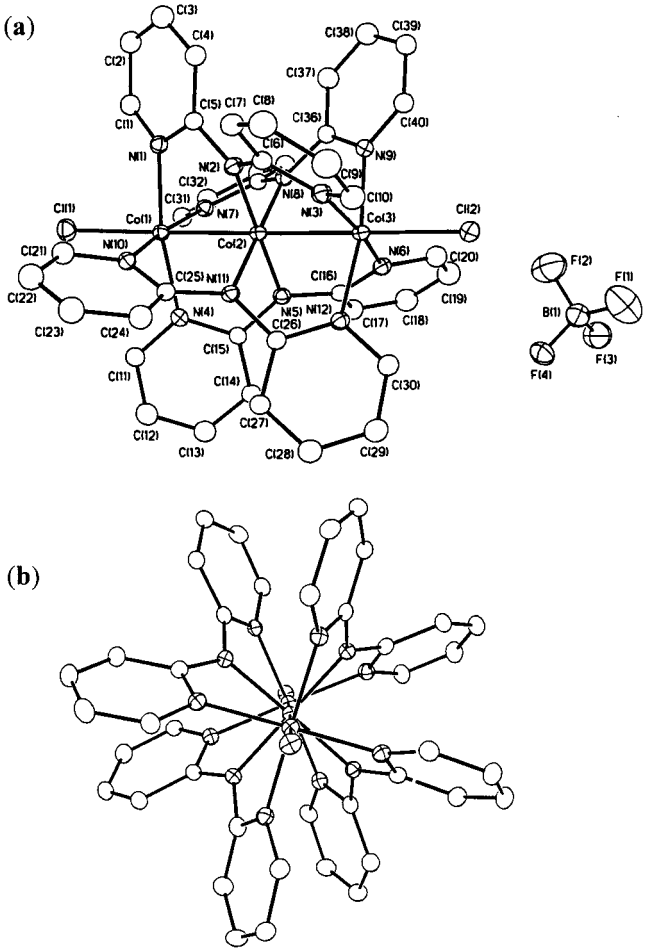

Figure 4. (a) Perspective view of $[Co_3(dpa)_4Cl_2][BF_4]$ in **2**·$2CH_2Cl_2$ at 213 K. Atoms are drawn at the 40% probability level and hydrogen atoms are omitted for clarity. (b) a view of the cation of **2** looking down the Co_3 axis.

Crystal Structure. Compound **2**·xCH_2Cl_2 crystallizes in the monoclinic space group $P2_1/n$ (see Table 1). The salt consists of the tricobalt cation $[Co_3(dpa)_4Cl_2]^+$ (**1**$^+$) and a $[BF_4]^-$ anion. A thermal ellipsoid plot of the cation in the 100 K data set is presented in Figure 4a, together with the atom-labeling scheme used. Distances and angles pertaining to the inner coordination of the Co atoms are listed in Table 2. The trinuclear Co_3^{7+} unit is supported by four dpa ligands in a spiral configuration as shown in Figure 4b. The Co−Co−Co unit is linear and essentially symmetrical. The cation **1**$^+$ resides on a general position with two independent Co−Co distances of 2.3168(8) and 2.3289(8) Å. Each of the terminal Co atoms is connected to a chlorine atom with a Co(1)−Cl(1) distance of 2.350(1) Å and a Co(3)−Cl(2) distance of 2.376(1) Å. The average Co−N distance for the terminal Co atoms is 1.977 Å and the mean central Co−N distance is 1.869 Å. As expected for a more highly charged metal ion, the average terminal Co−N and central Co−N distances are shorter (by 0.011 and 0.028 Å), relative to that of the neutral molecule **1**.[1b] The largest difference in bond lengths is found in the average axial Co−Cl distance, which is about 0.15 Å shorter in **1**$^+$ than that in **1**.[1b] Another factor contributing to a decrease in metal−ligand distances is the removal of one electron from an antibonding orbital of the neutral molecule of **1**. The fairly large decrease in the axial Co−Cl distance is consistent with a previous theoretical calculation[7] which revealed that the semioccupied molecular

(19) Cotton, F. A.; Murillo, C. A.; Wang, X. *Inorg. Chem.* **1999**, *38*, 6294−6297.

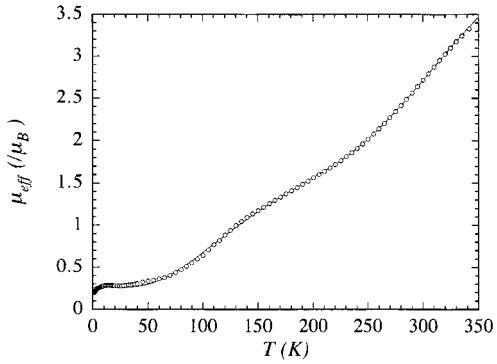

Figure 5. Temperature dependence of the effective magnetic moment measured in the solid state by direct magnetization measurement for **2**. (○, experimental data; −, fitted results).

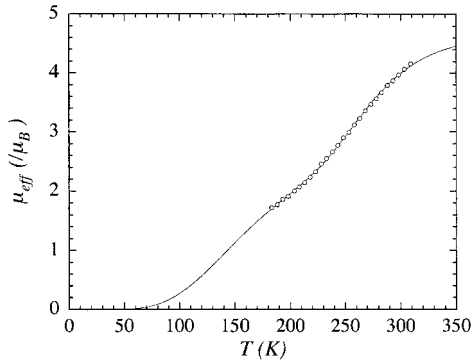

Figure 6. Temperature dependence of the effective magnetic moment measured in solution by the Evans method for **2** (○, experimental data; −, fitted results).

orbital (SOMO) of **1** is of metal nonbonding and chlorine antibonding character. It is therefore quite reasonable that a one-electron oxidation of **1** (which removes an electron from the Co−Cl antibonding orbital) would give a shorter Co−Cl distance.

The crystal structure of **2**·$x$$CH_2Cl_2$ was also determined at 213 and 300 K; selected bond distances and angles are listed in Table 2. There are only minor differences in the interatomic distances and angles compared to those at 100 K, despite the fact that a two-step spin transition process has occurred in the solid state (vide infra). The two Co−Co distances increase by about 0.01 Å to 2.325(1) and 2.341(1) Å at 300 K. The average Co−N distance of 1.992 Å represents a 0.015 Å increase of the coordination sphere of the cobalt atoms from the data set at 100 K. This change of metal−ligand distances for **2** is quite small compared to the increase of ca. 0.085 Å observed for mononuclear spin-crossover Co compounds.[20] The small changes in the metal coordination are likely due to the fact that the spin crossover is not complete at 300 K.

Magnetic Susceptibility Studies. (A) Solid State Measurements. The magnetic behavior of **2**·$x$$CH_2Cl_2$ in the solid state is presented in Figure 5 in the form of a plot of the effective magnetic moment (μ_{eff}) versus temperature (T). Between 1.8 and 50 K, the compound is essentially diamagnetic with only a small extrinsic paramagnetic impurity being observed. A fitting to a Curie−Weiss law ($C = 0.011$ emu CGS K mol^{-1}, $\theta = -2$ K) leads to the estimation of a 3% spin $S = 1/2$ impurity. As the temperature increases to 50 K, the effective moment begins to increase in a nonmonotonic manner. This unusual dependence, which is reproducible for different samples of **2**·$x$$CH_2Cl_2$, indicates the presence of a gradual two-step spin crossover. The gradual nature of this phenomenon, which is devoid of an intermediate plateau, implies a noncooperative spin crossover. This is confirmed by the lack of thermal hysteresis. At 350 K (the limit of the instrument), the effective moment gradually reaches a value of 3.45 μ_B with absence of saturation, which is evidence for an incomplete spin-crossover behavior.

(B) Solution Measurements. Figure 6 shows the effective magnetic moment of **2** calculated from the susceptibility measured by the Evans method in solution.[8] In the experimentally accessible temperature range of 183−309 K, the effective magnetic moment increases gradually from 1.72 to 4.16 μ_B. Although the experimental temperature range is limited, the shape of the curve (Figure 6) resembles the data obtained in the solid state. This result is quite important, as it confirms the molecular nature of the two-step spin crossover.

(C) Modeling of the Two-Step Spin Crossover Process. Two-step spin-crossover processes have been previously reported for several Fe(II) complexes.[21] Two explanations for a two-step spin crossover are found in the literature. The commonly accepted theory for Fe(II) complexes is an antiferromagnetic-type of interaction that results from the pairing of high-spin and low-spin species in a binary system without going through an intermediate spin state.[22] The two-step spin transition curve is characterized by one temperature, T_{sc} (where $\Delta G = 0$ and $T_{sc} = \Delta H/\Delta S$), corresponding to the point (sometimes a plateau) at which equal populations of high- and low-spin species exist. Various approximations to the two-step spin crossover processes involving mononuclear,[23] dinuclear,[24] and 1D chains of metal centers[25] have been proposed. In some cases, the Fe(II) ions reside on two crystallographically independent sites in a three-dimensional structure.[26] When the difference in metal coordination environments becomes substantial, the Fe(II) ions at the two sites may undergo LS ($S = 0$) ↔ HS ($S = 2$) transitions at two different temperatures and a two-step spin conversion is observed, as in the case of tris(4,4′-bis-1,2,4-triazole)iron(II) diperchlorate, $[Fe(brt)_3][ClO_4]_2$.[26] The very nature of these independent spin transitions precludes the involvement of an intermediate spin state.

One additional origin for a two-step spin transition is the existence of an intermediate spin state, but this has yet to be verified in mononuclear iron complexes. It can, however, be proposed in the present case for the metal−metal bonded tricobalt system. As previously reported, a calculation[7] of the electronic structure for the neutral molecule of $Co_3(dpa)_4Cl_2$ (**1**) suggested that the molecule possesses a $b_2^2e^4a_2$ ground state. The unpaired electron occupies the a_2 orbital, which is of metal

(20) (a) Heinze, K.; Huttner, G.; Zsolnai, L.; Schober, P. *Inorg. Chem.* **1997**, *36*, 5457−5469. (b) Wolny, J. A.; Rudolf, M. F.; Ciunik, Z.; Gatner, K.; Wolowiec, S. *J. Chem. Soc., Dalton Trans.* **1993**, 1611−1621. (c) Zarembowitch, J. *New J. Chem.* **1992**, *16*, 255−267. (d) Thuéry, P.; Zarembowitch, J. *Inorg. Chem.* **1986**, *25*, 2001−2008.

(21) (a) Spiering, H.; Kohlhaas, T.; Romstedt, N.; Hauser., A.; Bruns-Yilmaz, C.; Kusz, J.; Gütlich, P. *Coord. Chem. Rev.* **1999**, *192*, 629−647. (b) Romstedt, H.; Hauser, A.; Spiering, H. *J. Phys. Chem. Solids*. **1998**, *59*, 265−275. (c) Gütlich, P.; Jung, J.; Goodwin, H. A. *NATO-ASI Series E: Appl. Sci*. (Coronado, E., Ed.) **1996**, *321*, 327−378. (d) Gütlich, P.; Hauser, A.; Spiering, H. *Angew. Chem., Int. Ed. Engl*. **1994**, *33*, 2024−2054. (e) Boinnard, D.; Bousseksou, A.; Dworkin, A.; Savariault, J. M.; Varret, F.; Tuchagues, J. P. *Inorg. Chem.* **1994**, *33*, 271−281.

(22) Romstedt, H.; Spiering, H.; Gütlich, P. *J. Phys. Chem. Solids* **1998**, *59*, 1353−1362.

(23) Koudriavtsev, A. B. *Chem. Phys.* **1999**, *241*, 109−126 and references therein.

(24) (a) Bousseksou, A.; Varret, F.; Nasser, J. *J. Phys. I* **1993**, *3*, 1463−1473. (b) Real, J. A.; Bolvin, H.; Bousseksou, A.; Dworkin, A.; Kahn, O.; Varret, F.; Zarembowitch, J. *J. Am. Chem. Soc*. **1992**, *114*, 4650−4658.

(25) Linares, J.; Spiering, H.; Varret, F. *J. Eur. Phys. B.* **1999**, *10*, 271−275.

(26) Garcia, Y.; Kahn, O.; Rabardel, L.; Chansou, B.; Salmon, L.; Tuchages, J. P. *Inorg. Chem.* **1999**, *38*, 4663−4670 and references therein.

Scheme 2

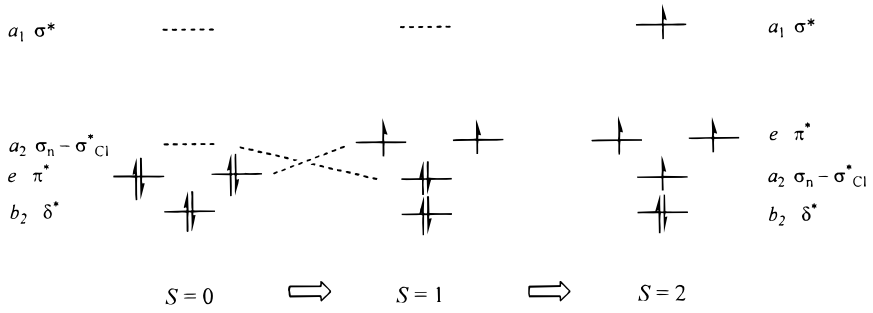

nonbonding and axial chlorine antibonding character. Oxidation of **1** removes the electron from the antibonding orbital and shortens the Co−Cl bond, as observed in the structure of the cation $\mathbf{1}^+$ in compound **2**. Thus **2** is expected to exhibit a diamagnetic $b_2^2e^4$ ground state as illustrated in Scheme 2.

As in the case of **1**, the small energy difference between the a_2 (LUMO) and e (HOMO) orbitals in **2** leads to a thermally accessible low-lying excited state. The difference in $\mathbf{1}^+$ versus **1** is that there are only two electrons available in $\mathbf{1}^+$ to occupy the doubly degenerate e orbital. This leads to an $S = 1$ excited state for **2**. At higher temperatures, the higher lying orbitals (possibly the metal-centered antibonding orbital a_1, the ligand antibonding orbitals, or a combination of both) can be populated to give an $S = 2$ species. Thus, the two-step spin transition for **2** involves a tertiary system (eq 2):

$$\underset{n_0}{(\mathbf{2})_{S=0}} \overset{K_1}{\longleftrightarrow} \underset{n_1}{(\mathbf{2})_{S=1}} \overset{K_2}{\longleftrightarrow} \underset{n_2}{(\mathbf{2})_{S=2}} \qquad (2)$$

where n_0, n_1, and n_2 are the number of moles for **2** in the solid state with a spin state of $S = 0$, $S = 1$, and $S = 2$, respectively. In solution, these values represent the corresponding molar concentrations. K_1 and K_2 are the equilibrium constants associated with the $S = 0 \leftrightarrow S = 1$ and $S = 1 \leftrightarrow S = 2$ spin-crossover processes, respectively. These constants are defined by the following ratios: $K_1 = n_1/n_0$ and $K_2 = n_2/n_1$.

The lack of thermal hysteresis and the gradual nature of the two-step spin-crossover curve for **2** allows the estimation of the enthalpy and entropy changes associated with the process, provided that intermolecular interactions both in the solid state and in solution are ignored. According to the mass action law of ideal solutions,[27] the effective magnetic moment can be expressed by

$$\mu_{\text{eff}}{}^2 = \frac{n_1}{n_t}\mu_1{}^2 + \frac{n_2}{n_t}\mu_2{}^2 \qquad (3)$$

where μ_{eff} is the measured effective magnetic moment, n_t is the total number of moles of **2** in the solid state or the total concentration of **2** in solution. The values μ_1 and μ_2 are molar magnetic moments for $S = 1$ and $S = 2$ species, respectively (since the magnetic moment μ_0 for the ground state of **2** is zero, it does not appear in eq 3). These values are 2.74 μ_B for μ_1 and 4.75 μ_B for μ_2, when the EPR experimental g factor of 1.94 is used. By introducing the equilibrium constants in eq 3 we have

$$\mu_{\text{eff}}{}^2 = \frac{\mu_1{}^2K_1 + \mu_2{}^2K_1K_2}{1 + K_1 + K_1K_2} \qquad (4)$$

(27) (a) Kahn, O. *Molecular Magnetism*; VCH: New York, 1993. (b) Gütlich, P.; Hauser, A. *Coord. Chem. Rev.* **1990**, *97*, 1−22. (c) Toftlund, H. *Coord. Chem. Rev.* **1989**, *94*, 67−108.

Considering the thermal dependence of the equilibrium constants,

$$K_i(T) = \exp\left(-\frac{\Delta H_i}{RT} + \frac{\Delta S_i}{R}\right) \qquad (5)$$

Equation 4 can be rewritten as

$$\mu_{\text{eff}}{}^2 = \left[\mu_1{}^2 \exp\left(-\frac{\Delta H_1}{RT} + \frac{\Delta S_1}{R}\right) + \mu_2{}^2 \exp\left(-\frac{\Delta H_1 + \Delta H_2}{RT} + \frac{\Delta S_1 + \Delta S_2}{R}\right)\right] / \left[1 + \exp\left(-\frac{\Delta H_1}{RT} + \frac{\Delta S_1}{R}\right) + \exp\left(-\frac{\Delta H_1 + \Delta H_2}{RT} + \frac{\Delta S_1 + \Delta S_2}{R}\right)\right] \qquad (6)$$

where ΔH_i and ΔS_i are the enthalpy and entropy changes associated with the equilibrium i.

Using eq 6, a least-squares fit of the thermal dependence of effective moment obtained in the solid state (Figure 5) and in solution (Figure 6) are in excellent agreement with the experimental measurements. In solution, the fitted thermodynamic parameters are $\Delta H_1 = 8.7$ kJ mol^{-1} and $\Delta S_1 = 43$ J mol^{-1} K^{-1}, for the singlet−triplet spin crossover, and $\Delta H_2 = 22.8$ kJ mol^{-1}, $\Delta S_2 = 81$ J mol^{-1} K^{-1}, for the triplet−quintet one. The characteristic temperature of 201 K is obtained from $T_{sc1} = \Delta H_1/\Delta S_1$ for the first step, while a significantly higher temperature of 281 K is found for the second step. The high-spin ($S = 2$) species is calculated to be 57% at 295 K, while the other intermediate spin ($S = 1$) and low spin ($S = 0$) species are 36% and 7%, respectively. In the solid state, these parameters are $\Delta H_1 = 3.6$ kJ mol^{-1}, $\Delta S_1 = 11$ J mol^{-1} K^{-1}, and $T_{sc1} = 315$ K for the first step, and $\Delta H_2 = 17.4$ kJ mol^{-1}, $\Delta S_2 = 53$ J mol^{-1} K^{-1}, $T_{sc2} = 330$ K for the second step. At 295 K the population of the different spin states are found to be 18%, 38%, and 44%, for $S = 2$, $S = 1$, and $S = 0$ spin states, respectively. This analysis is in good agreement with the observed similarities of the solid state structures at various temperatures. Since there is still a large fraction of the molecules with a singlet state at room temperature, the observed structural changes are expected to be very small. The two-step spin crossover proceeds further above room temperature in the solid state and it is still incomplete at the highest experimentally accessible temperature of 350 K. A similar trend is observed in solution, though the characteristic temperature is lower compared to that of the solid.

The data are in good agreement with reported data for Co^{II} spin-crossover complexes.[20] Any slight differences in the enthalpy and entropy values estimated from the solution and solid-state data can be attributed to the effect of crystal packing

forces which render it more difficult to access the higher spin state. To a first approximation, the ΔS term consists of three main contributions:[27]

$$\Delta S = \Delta S_{spin} + \Delta S_{solv} + \Delta S_{vib} \quad (7)$$

Here ΔS_{spin} denotes the entropy variation due to the increase of spin multiplicity (neglecting orbital contributions); ΔS_{solv} is the entropy change due to the difference of solvation at different spin states (to be considered only in solution); and ΔS_{vib} is the change of vibrational entropy because of the increase in bond length. The ΔS_{spin} contribution is usually assumed to be equal to $R \ln[(2S+1)_{HS}/(2S+1)_{LS}]$. Thus, the value of ΔS_{spin} would be $R \ln 3 = 9.1$ J mol^{-1} K^{-1} and $R \ln(5/3) = 4.2$ J mol^{-1} K^{-1} for $S = 0$ to $S = 1$ and $S = 1$ to $S = 2$ spin-crossover processes, respectively. The entropy changes from the data fits are found to be larger than the spin-only values. These discrepancies may be due to a higher density of vibrational states in the solid or to an increase in solvation for the high-spin species in solution. Since the overall size of the cation does not change significantly, the solvation component ΔS_{solv} will be negligible. Thus the major contribution to entropy changes in higher spin states is most likely due to the increased vibrational density as a result of weaker metal−metal or metal−ligand bonds or delocalization of the unpaired electrons on the ligand antibonding π^* orbitals. It should be noted, however, that the bond weakening resulting from spin crossover does not lead to dissociation of the ligands, as evidenced by the observed D_4 symmetry of the cation $[Co_3(dpa)_4Cl_2]^+$ in solution at room temperature.

Concluding Remarks

As far as we are aware, this study is the first documentation of a two-step spin crossover for a cobalt compound. Furthermore, it is the first case of a spin crossover that involves three spin states. The linear tricobalt compound **2** exhibits $S = 0$, 1, and 2 spin states over the temperature range of ~50−350 K. The results are rationalized on the basis of the molecular electronic structure that consists of a metal−metal bonded Co_3^{7+} unit. Detailed theoretical calculations for **2** are presently underway in our laboratory to understand, quantitatively, the change of electronic structures associated with this two-step spin crossover process.

Acknowledgment. The authors thank the National Science Foundation for financial support. We also acknowledge Professors Eugenio Coronado and Philipp Gütlich for helpful discussions.

Supporting Information Available: X-ray crystallographic data for compound **2** (CIF). This material is available free of charge via the Internet at http://pubs.acs.org.

JA994051B